ADVANCES IN ATMOSPHERIC SCIENCES, VOL. 38, FEBRUARY 2021, 307–316

• **Data Description Article** •

CAS-ESM2.0 Model Datasets for the CMIP6 Ocean Model Intercomparison Project Phase 1 (OMIP1)

Xiao DONG[1], Jiangbo JIN[*1], Hailong LIU[2,3], He ZHANG[1], Minghua ZHANG[1], Pengfei LIN[2], Qingcun ZENG[1], Guangqing ZHOU[4], Yongqiang YU[2,3], Mirong SONG[2], Zhaohui LIN[1], Ruxu LIAN[1], Xin GAO[1], Juanxiong HE[1], Dongling ZHANG[1], and Kangjun CHEN[2]

[1]*International Center for climate and Environment Sciences*, *Institute of Atmospheric Physics*, *Chinese Academy of Sciences*, *Beijing* 100029, *China*

[2]*State Key Laboratory of Numerical Modeling for Atmospheric Sciences and Geophysical Fluid Dynamics*, *Institute of Atmospheric Physics*, *Chinese Academy of Sciences*, *Beijing* 100029, *China*

[3]*College of Earth and Planetary Sciences*, *University of Chinese Academy of Sciences*, *Beijing* 100049, *China*

[4]*Institute of Atmospheric Physics*, *Chinese Academy of Sciences*, *Beijing* 100029, *China*

(Received 28 May 2020; revised 18 August 2020; accepted 4 September 2020)

ABSTRACT

As a member of the Chinese modeling groups, the coupled ocean–ice component of the Chinese Academy of Sciences' Earth System Model, version 2.0 (CAS-ESM2.0), is taking part in the Ocean Model Intercomparison Project Phase 1 (OMIP1) experiment of phase 6 of the Coupled Model Intercomparison Project (CMIP6). The simulation was conducted, and monthly outputs have been published on the ESGF (Earth System Grid Federation) data server. In this paper, the experimental dataset is introduced, and the preliminary performances of the ocean model in simulating the global ocean temperature, salinity, sea surface temperature, sea surface salinity, sea surface height, sea ice, and Atlantic Meridional Overturning Circulation (AMOC) are evaluated. The results show that the model is at quasi-equilibrium during the integration of 372 years, and performances of the model are reasonable compared with observations. This dataset is ready to be downloaded and used by the community in related research, e.g., multi-ocean–sea-ice model performance evaluation and interannual variation in oceans driven by prescribed atmospheric forcing.

Key words: OGCM, CMIP6, OMIP1, AMOC, ocean temperature/salinity, sea ice

Citation: Dong, X., and Coauthors, 2021: CAS-ESM2.0 model datasets for the CMIP6 Ocean Model Intercomparison Project Phase 1 (OMIP1). *Adv. Atmos. Sci.*, **38**(2), 307−316, https://doi.org/10.1007/s00376-020-0150-3.

1. Background

The ocean covers more than 70% of the entire surface of the Earth and contains more than 95% of the Earth's water that participates in the hydrological cycle. Besides, the ocean is also a large reservoir of heat owing to its large spatial extent and high heat capacity. Therefore, the ocean is an essential component of the Earth system and deserves intensive study. However, the scarcity of observational data in the ocean hampers its scientific research, especially for deep ocean waters and the Southern Ocean (Garuba and Klinger, 2016). Thus, ocean general circulation models (OGCMs) are essential tools in the scientific community, and are widely used to simulate the state and variation of the ocean. The outputs of OGCMs can also provide us with information where observational data are unavailable. Designing and conducting numerical experiments using OGCMs can help us to understand the evolution and mechanisms of ocean circulation.

Currently, there are large simulation spreads at centennial and longer time scales in the ocean modeling community (Griffies et al., 2009). To compare the behaviors of different ocean models and understand the origin of model biases in phase 6 of the Coupled Model Intercomparison Project (CMIP6), the Ocean Model Intercomparison Project (OMIP), an endorsed sub-project of CMIP6, was proposed (Griffies et al., 2016), which provides an experimental protocol for global ocean/sea-ice simulations forced with common atmospheric datasets. In the OMIP experiments, the ocean model is coupled with the sea-ice model forced by prescribed atmospheric fields. There are 11 model groups participating in the OMIP experiments according to Tsujino et

* Corresponding author: Jiangbo JIN
Email: jinjiangbo@mail.iap.ac.cn

al. (2020). The Co-ordinated Ocean–Ice Reference Experiment II (CORE II) datasets (Large and Yeager, 2009) are applied to force the global ocean/sea-ice models, which is denoted as phase 1 of the physical part of OMIP (OMIP1). Recently, a new OMIP experiment has been proposed, applying Japanese 55-year Reanalysis (JRA-55; Kobayashi et al., 2015) to drive the ocean–ice model, which is denoted as OMIP2. The period covered by the JRA-55 datasets is 1958–2018. The OMIP experiments are regarded as a fundamental test for ocean modelers (Griffies et al., 2016). Because the OMIP1 experiments are conducted by the ocean–ice coupled model component of the Chinese Academy of Sciences' Earth System Model, version 2.0 (CAS-ESM2.0), we mainly focus on OMIP1 in this paper.

CAS-ESM2.0, which will take part in CMIP6, is a newcomer in the modeling community (Zhang et al, 2020). The ocean component of CAS-ESM2.0 is a revised version of the State Key Laboratory of Numerical Modeling for Atmospheric Sciences and Geophysical Fluid Dynamics/Institute of Atmospheric Physics (LASG/IAP) Climate Ocean Model, version 2 (LICOM2.0) (Liu et al., 2012). The coupled ocean–ice component of CAS-ESM2.0 will participate in the OMIP1 experiment, and datasets will be released to CMIP6 for researchers worldwide. Here, a baseline evaluation of the coupled ocean–ice component of CAS-ESM2.0 in the OMIP1 experiment is presented.

The remainder of the paper is structured as follows: Section 2 describes the model and experimental design; section 3 gives a basic technical validation of OMIP1; a summary is provided in section 4; and section 5 offers usage notes.

2. Model and experiment

The ocean component of CAS-ESM2.0 is based on LICOM2.0 (Liu et al., 2012). In LICOM2.0, the horizontal resolution is approximately 1° globally, except for a finer resolution of 0.5° between 10°S and 10°N. This resolution can resolve the equatorial waves and capture the upper mixed layer and thermocline (Lin et al., 2013, 2016, 2020). There are 30 levels in the vertical direction, with 10 m per layer in the upper 150 m, and the depths of the W-grid and T-grid are shown in Table 1. This model considers three key physical processes: (1) a second-order turbulent mixing scheme (Canuto et al., 2001, 2002); (2) a solar radiation penetration scheme based on chlorophyll-a (Ohlmann, 2003); and (3) a mesoscale eddy parameterization from Gent and McWilliams (1990). Besides, compared to the original version of LICOM2.0, key improvements have been made as follows:

(1) A new sea surface salinity (SSS) boundary condition has been introduced based on the physical process of air–sea flux exchange at the actual sea–air interface, rather than the commonly used virtual salt flux scheme. The new scheme can reproduce the magnitude of Atlantic Meridional Overturning Circulation (AMOC) better than the original one (Jin et al., 2017).

(2) The diurnal variation of sea surface temperature (SST) is resolved by coupling the atmospheric and oceanic model components once every two hours.

(3) A new formulation of turbulent air–sea fluxes (Fairall et al., 2003) has been introduced, which improves the latent heat flux and wind stress simulations. In the new scheme, the effects of gustiness are parameterized, and the thermal stability of the marine atmosphere boundary layer is considered in detail (Pelletier et al., 2018).

The sea-ice model in CAS-ESM2.0 is an improved Los Alamos sea-ice model, version 4.0 (Hunke and Lipscomb, 2008), using the same grid as the oceanic model. The model solves the dynamic and thermodynamic equations for five ice thickness categories, with one snow layer and four ice layers. For the dynamic component, the model uses elastic–viscous–plastic rheology (Hunke and Dukowicz, 1997), a mechanical redistribution scheme (Lipscomb et al., 2007), and an incremental remapping advection scheme (Lipscomb and Hunke, 2004). For the thermodynamic component, a parameterization with a relatively more realistic sea-ice salinity budget (Liu, 2010) is used. Also employed is an improved CCSM3 radiation scheme for the albedo and radiative fluxes at the sea-ice surface, which works by incorporating explicit melt ponds and their impact on albedo, expanding the spectrum from two to four bands, distinguishing direct and diffuse short waves, and considering different albedos for wet and dry snow, as well as sea-ice and snow thickness effects on albedo.

The OMIP1 experiment follows the CORE-II protocol, and the initial conditions of the coupled ocean–ice component of CAS-ESM2.0 are from the World Ocean Atlas (Antonov et al., 2006, 2010) temperature and salinity and state of rest. The SSS is restored to monthly climatological observations from the World Ocean Atlas (Antonov et al., 2006, 2010), with a restoring velocity of 50 m $(4\ \mathrm{yr})^{-1}$ for the sea surface and 50 m $(30\ \mathrm{d})^{-1}$ for the sea ice.

The forcing fields in OMIP1 are CORE-II datasets, which are mainly derived from the NCEP–NCAR atmospheric reanalysis. The forcing dataset covers the 62-year period from 1948 to 2009, and the temporal resolution of CORE-II is 6 hours and the horizontal resolution is T62. The atmospheric forcing from the CORE-II datasets, including atmospheric wind vectors at 10 m, surface air temperature at 10 m, specific humidity at 10 m, air density at 10 m, precipitation including rain and snow, surface downward shortwave and longwave radiation, sea level pressure, and runoff, is prescribed. To derive quasi-equilibrium and stable results, the ocean–sea ice coupled model is integrated for 372 years (six cycles of the CORE-II period). In the following section, we present a baseline evaluation of the OMIP1 simulation by the coupled ocean–ice component of CAS-ESM2.0.

3. Technical validation

A preliminary evaluation of the performance in the OMIP1 experiment by the coupled ocean–ice component of CAS-ESM2.0 is provided in this section, including the temporal evolution and spatial pattern of global mean ocean temperature, sea ice, and the AMOC, which are essential met-

rics to evaluate the behaviors of the coupled ocean–ice model. In the final subsection (i.e., 3.6), a brief discussion comparing the behaviors of the ocean–sea ice model and the fully coupled model (i.e., CAS-ESM2.0), is presented. The following observational datasets are used to evaluate the model performances: The annual mean ocean temperature and salinity are from the World Ocean Atlas 2013 (Boyer et al., 2013). The observed sea surface height (SSH) is from AVISO (Archiving, Validation and Interpretation of Satellite Oceanographic Data; http://www.aviso.altimetry.fr/). The sea-ice data are from the Meier et al. (2017) NOAA climate data record ice extent. The observed vertical profiles of the time-averaged AMOC at 26.5°N are from the RAPID (The Rapid Climate Change programme) observations (Cunningham et al., 2007; McCarthy et al., 2015; Smeed et al., 2018).

3.1. *Global mean*

First, to evaluate the stability of the ocean model integration, the time series of global annual mean temperature and salinity at the surface and throughout the whole ocean are shown in Fig. 1. The model integration covers 372 years, including 6 cycles of the observational period of 62 years (1948–2009). This cyclic feature is clear in the global mean SST and SSS. Signatures of interannual variations are also apparent at the sea surface, with temperature (salinity) fluctuating at approximately 18.40°C (34.7–34.8 psu). The global mean SST and SSS at the mean time of the final cycle is 18.41°C and 34.73 psu, respectively, and the corresponding observational values are 18.39°C and 34.73 psu. For the global volume-averaged ocean temperature (VOT), the simulated VOT shows a near stationary state (~3.83°C) throughout the entire integration, indicating that the model reaches quasi-equilibrium and that the drift of sea surface heat flux can be negligible.

We also provide the time series of the AMOC maximum at 26.5°N in the full integration. The time series exhibits an evident period of 62 years, similar to the time series of SST and SSS. This feature can be reasonably reproduced by the model in each atmospheric forcing cycle. The drift is very small after the adjustment of the first cycle, which further confirms the stability of the model integration. The simulated magnitude of the AMOC maximum at 26.5°N at the mean time of the final cycle is approximately 17.7 Sv (Sv = 10^6 m^3 s^{-1}).

3.2. *Spatial patterns*

Figure 2 shows the spatial patterns of SST and SSS biases compared with observations. The last 30 years of integration is shown. In general, the model can reasonably reproduce the global patterns of SST and SSS. The global mean biases of SST and SSS are 0.07°C and 0.04 psu, respectively. The simulated SST bias exhibits common anomalous patterns in many climate models (Golaz et al., 2019; Held et al., 2019), with opposite signs between sub-polar regions (a prominent colder bias in the Arctic Ocean and warmer bias in the Southern Ocean). Overall warm biases are found in coastal upwelling regions, such as the western coasts of the

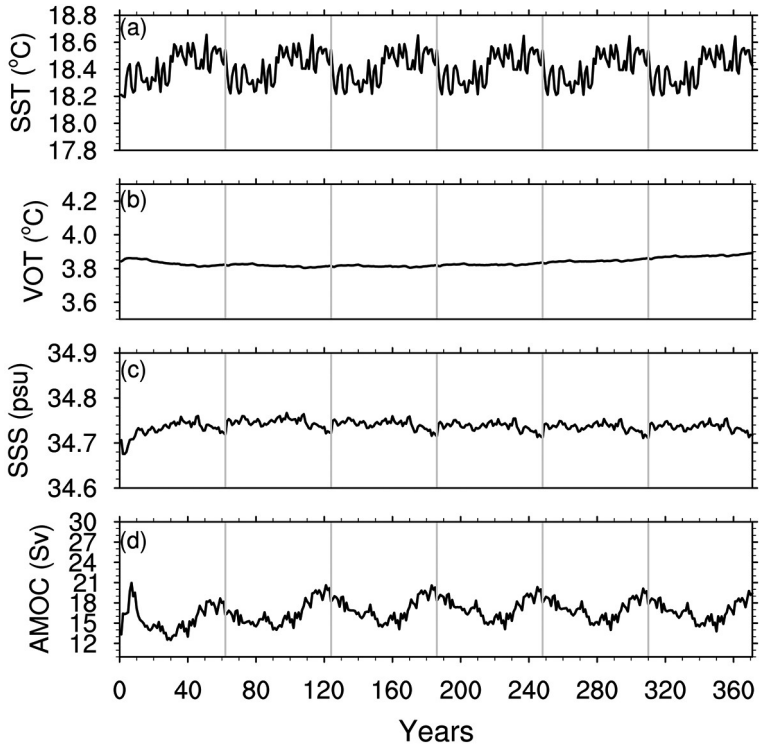

Fig. 1. Time series of global annual mean (a) SST, (b) VOT, (c) SSS, and (d) AMOC maximum values at 26.5°N in the CAS-ESM2.0 OMIP1 experiment. The six cycles are separated by vertical gray lines.

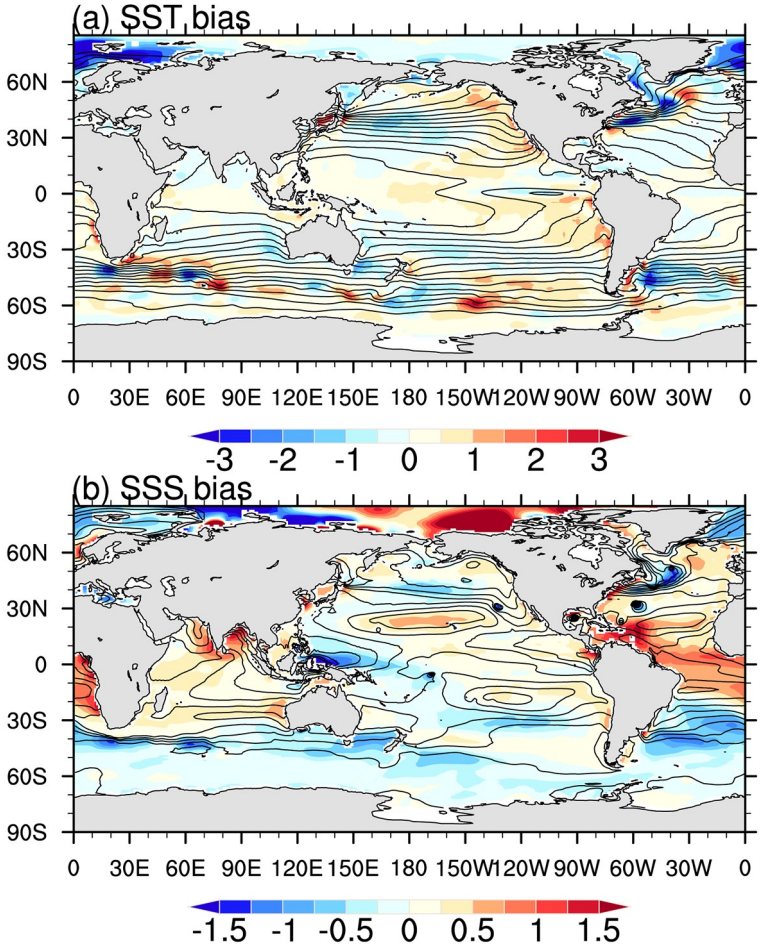

Fig. 2. Spatial pattern of simulated bias in (a) SST (units: °C) and (b) SSS (units: psu); the contours in (a, b) are simulated SST and SSS values, respectively. The simulation time mean is taken from the last 30 years of integration.

continents of America and Africa, and the eastern equatorial Pacific, which may be associated with poorly resolved coastal upwelling due to coarse grid resolution. Cold anomalies are mainly concentrated in subtropical regions, especially the margins of western currents. For the SSS bias, the freshwater bias is in the high latitudes and western equatorial Pacific, while the saline water SSS bias is located in the tropical Atlantic Ocean and Beaufort Sea in the Arctic Ocean. The root-mean-square errors of SST and SSS are 0.65°C and 0.49 psu, respectively.

The observed and simulated climatological annual mean SSH are shown in Fig. 3. The simulation can reasonably capture the spatial features of SSH from observations, with a large pattern correlation coefficient of 0.96 between them. In both the simulation and observation, the high SSHs are located around the western boundary in the low and middle latitudes of the Pacific and Atlantic oceans in both hemispheres, while the low ones are close to the eastern boundary, which is associated with the westward ocean currents and trade winds. In addition, a salient asymmetric feature exists; namely, a ridge of SSH in the northern western Pacific that is higher than its counterpart in the Southern Hemisphere. In the Indian Ocean, the east–west contrast reverses in the tropical region, with higher SSH located in the east and lower in the west. In high latitudes, the relatively low SSHs are located in the subpolar gyre in the Northern Hemisphere. The lowest SSHs in the global ocean are located around the Antarctic Circumpolar Current in the Southern Ocean.

3.3. *Zonal mean*

We further show the distribution of the zonal mean ocean temperature and salinity biases of different basins in Fig. 4, derived from the last 30 years of integration. The global ocean is divided into three basins: the Southern Ocean (78°S–35°N); the Indo-Pacific Ocean (35°S–65°N, 22°–134°E); and the Arctic and Atlantic oceans (35°S–90°N). In the Southern Ocean, the zonal mean temperature bias exhibits a south-warm–north-cold dipole pattern in the upper 1000 m. Below 1000 m, the model simulation shows a warm bias. In the Indo-Pacific basin, the pattern of the warm bias in the North Pacific has its largest bias at depths of 100–200 m, and the surface cold bias in its southern region expands downward and dominates the entire

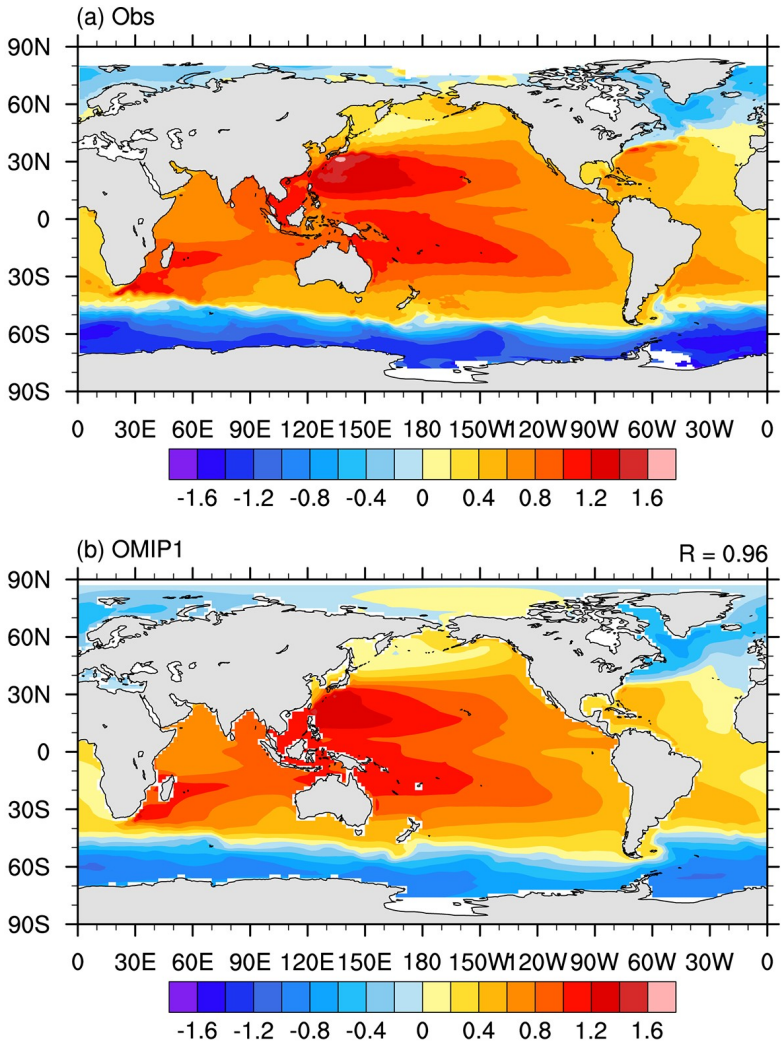

Fig. 3. Climatological annual mean SSH (units: m) in the (a) observations and (b) CAS-ESM2.0 OMIP1 simulation. The pattern correlation coefficient between the observations and simulation is shown in the top-right corner in panel (b).

basin below 1000 m. With respect to the Atlantic–Arctic Ocean basin, it generally shows an overly warm bias, especially from the depth of 600 to 3000 m, with freshwater biases in the Arctic Ocean in the upper 300 m (Fig. 4b). Compared to that in the Atlantic–Arctic Ocean basin, the salinity bias in the Southern Ocean and Indo-Pacific Ocean basin is minimal. Most ocean areas in the Southern Ocean and Indo-Pacific Ocean have positive salinity biases, except in the upper northern region in the Southern Ocean and subsurface tropical Indo-Pacific regions, where cold biases occur (Fig. 4b).

3.4. *AMOC*

In the Atlantic, the most active thermohaline circulation occurs in the global ocean, which can be represented by the AMOC. The AMOC can portray the transport of volume or mass in the Atlantic. AMOC simulation is one of the key indicators used to measure the performance of an ocean model. Figure 5a shows the AMOC simulation in the ocean component of CAS-ESM2.0 over the final decade (2000–09) mean of the final cycle. The model can reasonably reproduce the North Atlantic Deep Water (NADW) between 500 m and 3000 m north of 35°S, and the Antarctic Bottom Water below 3000 m. Compared with the observations at 26.5°N, the model can simulate the peak value at the right depth of approximately 1000 m, with magnitudes up to 18.6 Sv, which is slightly greater than the 18.3 Sv inferred from observations for 2004–09 (Cunningham et al., 2007; Smeed et al., 2018). The simulated AMOC depth is largely limited to the top 3000 m, which is slightly shallower than the 4300 m in observational estimates (McCarthy et al., 2015).

3.5. *Sea ice*

In the OMIP experiment, the sea-ice model is coupled with the ocean model and can interact with the ocean model; thus, the sea-ice concentration (SIC) is another metric used to evaluate the model results. Figure 6 shows the spa-

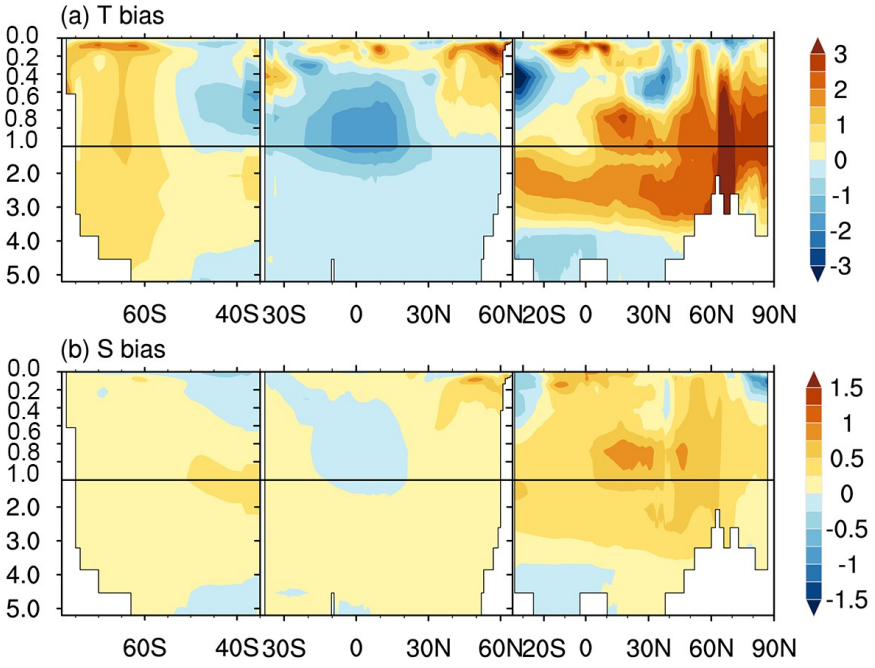

Fig. 4. Latitude–depth plot of the zonal mean (a) ocean temperature bias (units: °C) and (b) salinity bias (unit: psu) in the Southern Ocean, Indo-Pacific Ocean, and Atlantic–Arctic Ocean basins. The simulation time mean is taken from the last 30 years of integration. The unit on the *y*-axis is km.

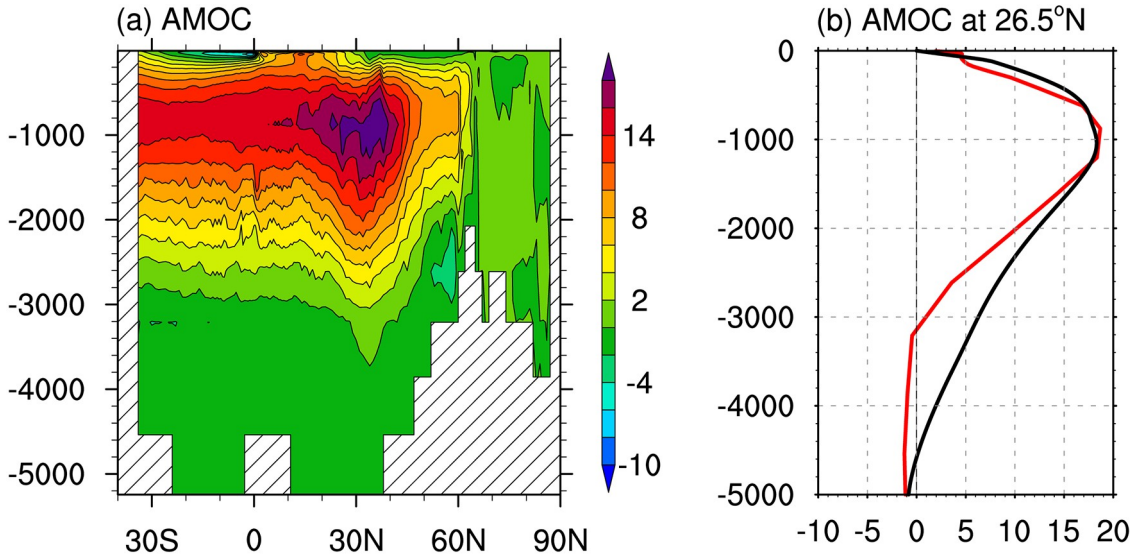

Fig. 5. (a) The AMOC stream function (units: Sv) averaged over the last 10 years of integration. (b) Vertical profiles of the time-averaged circulation at 26.5°N in the simulation (red) and observations (black).

tial pattern and temporal evolution of the simulated sea-ice area in the Arctic and Antarctic. The coupled ocean and sea-ice model can reasonably reproduce the SIC in both the Northern and Southern hemispheres (Figs. 6a–d). For the wintertime in both hemispheres (March in the Northern Hemisphere and September in the Southern Hemisphere), the SIC is overestimated in the Iceland and Bering seas in the Northern Hemisphere and almost the entire Antarctic region in the Southern Hemisphere, as indicated by the difference in the black and purple contours that represent the threshold of 15% coverage. Similarly, the slightly underestimated SIC in summertime in both hemispheres (September in the Northern Hemisphere and March in the Southern Hemisphere) is mainly located in the Chukchi Sea, East Siberian Sea, Laptev Sea, Canada basin, Ross Sea, and Weddell Sea. Figure 6e provides the time series of the maximum and minimum sea-ice areas in both hemispheres, which is also an important measure to show the stability of the model dur-

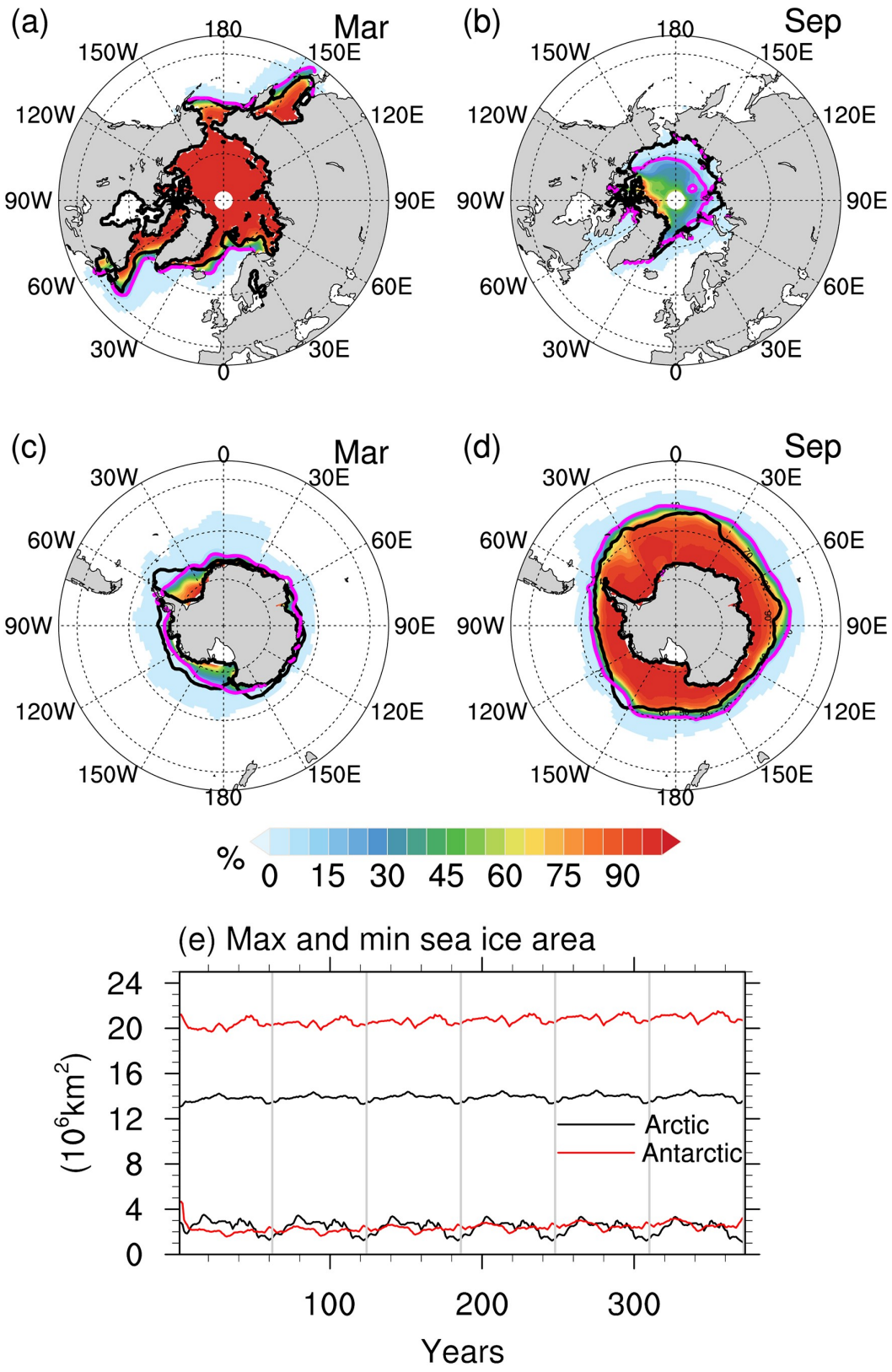

Fig. 6. (a–d) Spatial patterns of the simulated SIC in (a, c) March and (b, d) September, in (a, b) the Northern Hemisphere and (c, d) the Southern Hemisphere. The thick black (purple) line denotes the 15% contour line in the observations (simulation). The simulation time mean is taken from the last 30 years of integration. (e) Time series of the maximum and minimum of the total sea-ice area for the Arctic and Antarctic in the simulation (units: 10^6 km^2). The black (red) line denotes the Arctic (Antarctic). The six cycles are separated by vertical gray lines.

ing integration. The simulated sea-ice area in the two hemispheres drifts minimally in the seasonal cycle of the sea-ice area during the whole integration, with interannual variation and 62-year atmospheric forcing cycles. In addition, it is obvious that the difference between the maximum and minimum sea-ice areas is larger in the Antarctic than in the Arctic, which indicates a larger seasonal cycle in the Antarctic than in the Arctic.

3.6. *Comparison of coupled model behaviors*

According to the above results, the behaviors of the coupled ocean–ice model forced by prescribed CORE-II data can reasonably reproduce the preliminary performances of the ocean. In addition to the OMIP1 experiment, CAS-ESM2.0 also conducted the CMIP6 historical experiment (see footnote). Understanding the behaviors in standalone component models is an essential part of investigating the bias of the fully coupled model. Actually, on the whole, the ocean–ice model has similar bias patterns as the coupled model simulation, indicating to some extent that the coupled simulation bias has some origin in the ocean model. Taking the zonal mean temperature simulation as an example, the coupled model also has a warm bias throughout the South Indian Ocean, in the upper level of the North Pacific Ocean, and in the NADW, and a cold bias at depths of ~800 m in the North Indian Ocean and tropical Pacific Ocean, as the ocean model shows in Fig. 4. In some respects, the bias in the ocean model is decreased compared with the results from the coupled model, e.g., the subsurface cold biases in the Pacific Ocean and Indian Ocean are substantially reduced in the ocean model compared with the coupled model, suggesting that the bias in the atmospheric variables in the coupled model can enlarge the ocean model bias through air–sea coupling. Systematic evaluation of the coupled simulation of CAS-ESM2.0 has been provided in Zhang et al. (2020).

4. Summary

In this paper, the OMIP1 experiment outputs simulated by the coupled ocean–sea ice model in CAS-ESM2.0 have been introduced, and a basic evaluation of the model behaviors presented. The global mean time series of several key variables are provided to confirm the stabilization of the model integration. Then, the horizontal and vertical distributions of the model biases of temperature and salinity are also examined. The simulated spatial pattern of SSH is quite similar to observed, with a pattern correlation coefficient of 0.96. In general, the model can reasonably reproduce the general features of the ocean state, along with some common biases shared by most ocean–sea ice models (Griffies et al., 2009), such as the cold bias in the eastern Pacific cold tongue and the Arctic Ocean, the warm biases off the east coast of the basins and in the Southern Ocean. For AMOC, compared with the observations at 26.5°N, the model can capture the peak value at the right depth of approximately 1000 m, with magnitudes up to 18.6 Sv, which is slightly greater than observed (18.3 Sv). Finally, the sea-ice simulations in both hemispheres are presented. The SIC is slightly overestimated in wintertime and underestimated in summertime in both hemispheres, indicating a stronger seasonal cycle in the model.

5. Usage notes

The simulation data have been uploaded onto the Earth System Grid Federation (ESGF) data server for CMIP6 users to download, and can be found at https://esgf-node.llnl.gov/projects/cmip6/. The dataset format is NetCDF, version 4. The horizontal grid numbers of the model outputs are 360 and 196 in the zonal and meridional directions, respectively. The horizontal resolution is 1° in the extratropical regions (north to 20°N and south to 20°S) in the two hemispheres, with a finer resolution of 0.5° between 10°S and 10°N. The dataset has 30 vertical levels, with 10 m per layer in the upper 150 m, and the depths of the W-grid and T-grid are shown in Table 1. The original horizontal resolutions and vertical levels are not changed on the ESGF nodes, and all variables share the same grid. The variables of Priority 1 for OMIP are shown in Table 2, and the fre-

Table 1. T and W grids denote different variables locations in the vertical grid, the temperature *T*, salinity *S* and horizonal vectors (*u*, *v*) are located in T grid, and the vertical velocity *W* and pressure *P* are located in W grids. Negative value is the depth below Level 1 of W grid. (Units: m).

Level	Depth for T grid	Depth for W grid
1	−5	0
2	−15	−10
3	−25	−20
4	−35	−30
5	−45	−40
6	−55	−50
7	−65	−60
8	−75	−70
9	−85	−80
10	−95	−90
11	−105	−100
12	−115	−110
13	−125	−120
14	−135	−130
15	−145	−140
16	−156.9303	−150
17	−178.4277	−163.8606
18	−222.5018	−192.9948
19	−303.1057	−252.0088
20	−432.5961	−354.2027
21	−621.1931	−510.9896
22	−876.5334	−731.3966
23	−1203.337	−1021.67
24	−1603.2	−1385.003
25	−2074.526	−1821.396
26	−2612.596	−2327.656
27	−3209.772	−2897.536
28	−3855.835	−3522.009
29	−4538.428	−4189.662
30	−5243.597	−4887.194
31	–	−5600

Table 2. Descriptions of Priority 1 dataset variables for OMIP.

Name	Description	Units
hfbasin	Northward ocean heat transport	W
hfbasinpmadv	Northward ocean heat transport due to parameterized mesoscale advection	W
hfds	Downward heat flux at sea water surface	W m^{-2}
mlotst	Ocean mixed-layer thickness defined by sigma T	m
msftbarot	Ocean barotropic mass streamfunction	Sv = 10^6 m^3 s^{-1}
msftmz	Ocean meridional overturning mass streamfunction	Sv = 10^6 m^3 s^{-1}
obvfsq	Square of Brunt–Vaisala frequency in sea water	s^{-2}
pbo	Seawater pressure at sea floor	Pa
so	Seawater salinity	psu
sob	Seawater salinity at sea floor	psu
soga	Global mean sea water salinity	psu
sos	SSS	psu
sosga	Global average SSS	psu
thetao	Seawater potential temperature	°C
thetaoga	Global average sea water potential temperature	°C
tob	Seawater potential temperature at sea floor	°C
tos	SST	°C
tosga	Global average SST	°C
uo	Seawater X velocity	m s^{-1}
umo	Ocean mass X transport	kg s^{-1}
vo	Sea water Y velocity	m s^{-1}
wo	Seawater vertical velocity	m s^{-1}
wmo	Upward ocean mass transport	kg s^{-1}
zos	SSH above geoid	m

quency of variables is monthly, covering the period of 1–372 years (six cycles of the forcing data).

Acknowledgements. We greatly appreciate the constructive comments and suggestions from the two reviewers and Executive Editors-in-Chief. This work was jointly supported by the National Natural Science Foundation of China (Grant Nos. 41706036 and 41706028), the Key Research Program of Frontier Sciences, Chinese Academy of Sciences (Grant No. QYZDY-SSW-DQC002), the National Key R&D Program for Developing Basic Sciences (Grant Nos. 2016YFC1401401 2016YFC1401601 and 2016YFB0200804), the National Key Scientific and Technological Infrastructure project entitled "Earth System Science Numerical Simulator Facility" (EarthLab) and key operation construction projects of Chongqing Meteorological Bureau-"Construction of chongqing short-term climate numerical prediction platform".

REFERENCES

Antonov, J. I., and Coauthors, 2010: *Salinity*. Volume 2, *World Ocean Atlas 2009*. NOAA Atlas NESDIS 69.

Antonov, J. I., R. A. Locarnini, T. P. Boyer, A. V. Mishonov, and H. E. Garcia, 2006: *Salinity*. Volume 2, *World Ocean Atlas 2005*.NOAA Atlas NESDIS 61.

Boyer, T. P., and Coauthors, 2013: World Ocean Database 2013. NOAA Atlas NESDIS 72, 209 pp, http://doi.org/10.7289/V5NZ85MT.

Canuto, V. M., A. Howard, Y. Cheng, and M. S. Dubovikov, 2001: Ocean turbulence. Part I: One-point closure model—Momentum and heat vertical diffusivities. *J. Phys. Oceanogr.*, **31**, 1, https://doi.org/10.1175/1520-0485(2001)031<1413:OTPIOP>2.0.CO;2.

Canuto, V. M., A. Howard, Y. Cheng, and M. S. Dubovikov, 2002: Ocean turbulence. Part II: Vertical diffusivities of momentum, heat, salt, mass, and passive scalars. *J. Phys. Oceanogr.*, **32**, 240–264, https://doi.org/10.1175/1520-0485(2002)032<0240:OTPIVD>2.0.CO;2.

Cunningham, S. A., and Coauthors, 2007: Temporal variability of the Atlantic meridional overturning circulation at 26.5 N. *Science*, **317**, 935–938, https://doi.org/10.1126/science.1141304.

Fairall, C. W., E. F. Bradley, J. E. Hare, A. A. Grachev, and J. B. Edson, 2003: Bulk parameterization of air-sea fluxes: Updates and verification for the COARE algorithm. *J. Climate*, **16**, 571–591, https://doi.org/10.1175/1520-0442(2003)016<0571:BPOASF>2.0.CO;2.

Garuba, O. A., and B. A. Klinger, 2016: Ocean heat uptake and interbasin transport of the passive and redistributive components of surface heating. *J. Climate*, **29**, 7 507–7 527, https://doi.org/10.1175/JCLI-D-16-0138.1.

Gent, P. R., and J. C. McWilliams, 1990: Isopycnal mixing in ocean circulation models. *J. Phys. Oceanogr.*, **20**, 150–155,

https://doi.org/10.1175/1520-0485(1990)020<0150:IMIOCM>2.0.CO;2.

Golaz, J.-C., and Coauthors, 2019: The DOE E3SM coupled model version 1: Overview and evaluation at standard resolution. *Journal of Advances in Modeling Earth Systems*, **11**, 2 089–2 129, https://doi.org/10.1029/2018MS001603.

Griffies, S. M., and Coauthors, 2009: Coordinated ocean-ice reference experiments (COREs). *Ocean Modelling*, **26**, 1–46, https://doi.org/10.1016/j.ocemod.2008.08.007.

Griffies, S. M., and Coauthors, 2016: OMIP contribution to CMIP6: Experimental and diagnostic protocol for the physical component of the Ocean Model Intercomparison Project. *Geosci. Model Dev.*, **9**, 3 231–3 296, https://doi.org/10.5194/gmd-9-3231-2016.

Held, I. M. and Coauthors, 2019: Structure and performance of GFDL's CM4.0 climate model. *Journal of Advances in Modeling Earth Systems*, **11**, 3 691–3 727, https://doi.org/10.1029/2019MS001829.

Hunke, E. C., and J. K. Dukowicz, 1997: An elastic—viscous-plastic model for sea ice dynamics. *J. Phys. Oceanogr.*, **27**, 1 849–1 867, https://doi.org/10.1175/1520-0485(1997)027<1849:AEVPMF>2.0.CO;2.

Hunke, E. C., and W. H. Lipscomb, 2008: CICE: The Los Alamos Sea Ice Model User's Manual, Version 4. Los Alamos National Laboratory Tech. Rep. LA-CC-06-012, 76 pp.

Jin, J. B., Q. C. Zeng, L. Wu, H. L. Liu, and M. H. Zhang, 2017: Formulation of a new ocean salinity boundary condition and impact on the simulated climate of an oceanic general circulation model. *Science China Earth Sciences*, **60**, 491–500, https://doi.org/10.1007/s11430-016-9004-4.

Kobayashi, S. and Coauthors, 2015: The JRA-55 Reanalysis: General Specifications and Basic Characteristics. *J. Meteor. Soc. Japan*, **93**, 5–48, https://doi.org/10.2151/jmsj.2015-001.

Large, W. G., and S. G. Yeager, 2009: The global climatology of an interannually varying air-sea flux data set. *Climate Dyn.*, **33**, 341–364, https://doi.org/10.1007/s00382-008-0441-3.

Lin, P. F., Y. Q. Yu, and H. L. Liu, 2013: Long-term stability and oceanic mean state simulated by the coupled model FGOALS-s2. *Adv. Atmos. Sci.*, **30**, 175–192, https://doi.org/10.1007/s00376-012-2042-7.

Lin, P. F., and Coauthors, 2016: A coupled experiment with LICOM2 as the ocean component of CESM1. *J. Meteor. Res.*, **30**(1), 76–92, https://doi.org/10.1007/s13351-015-5045-3.

Lin, P. F., and Coauthors, 2020: LICOM Model datasets for CMIP6 Ocean Model Intercomparison Project (OMIP). *Adv. Atmos. Sci.*, **37**(3), 239–249, https://doi.org/10.1007/s00376-019-9208-5.

Lipscomb, W. H., and E. C. Hunke, 2004: Modeling sea ice transport using incremental remapping. *Mon. Wea. Rev.*, **132**, 1 341–1 354, https://doi.org/10.1175/1520-0493(2004)132<1341:MSITUI>2.0.CO;2.

Lipscomb, W. H., E. C. Hunke, W. Maslowski, and J. Jakacki, 2007: Ridging, strength, and stability in high-resolution sea ice models. *J. Geophys. Res. Oceans*, **112**, C03S91, https://doi.org/10.1029/2005JC003355.

Liu, H. L., P. F. Lin, Y. Q. Yu, and X. H. Zhang, 2012: The baseline evaluation of LASG/IAP climate system ocean model (LICOM) version 2. *Acta Meteorologica Sinica*, **26**, 318–329, https://doi.org/10.1007/s13351-012-0305-y.

Liu, J. P., 2010: Sensitivity of sea ice and ocean simulations to sea ice salinity in a coupled global climate model. *Science China Earth Sciences*, **53**, 911–918, https://doi.org/10.1007/s11430-010-0051-x.

McCarthy, G. D., and Coauthors, 2015: Measuring the Atlantic Meridional overturning circulation at 26 N. *Progress in Oceanography*, **130**, 91–111, https://doi.org/10.1016/j.pocean.2014.10.006.

Meier, W., F. Fetterer, R. Duerr, M. J. Stroeve, Savoie, and S. Mallory, 2017: NOAA/NSIDC climate data record of passive microwave sea ice concentration, Version 3. Available from https://doi.org/10.7265/N59P2ZTG.

Ohlmann, J. C., 2003: Ocean radiant heating in climate models. *J. Climate*, **16**, 1 337–1 351, https://doi.org/10.1175/1520-0442-16.9.1337.

Pelletier, C., F. Lemarié, and E. Blayo, 2018: Sensitivity analysis and metamodels for the bulk parametrization of turbulent air-sea fluxes. *Quart. J. Roy. Meteor. Soc.*, **144**, 658–669, https://doi.org/10.1002/qj.3233.

Smeed, D. A., and Coauthors, 2018: The North Atlantic Ocean is in a state of reduced overturning. *Geophys. Res. Lett.*, **45**, 1 527–1 533, https://doi.org/10.1002/2017GL076350.

Tsujino, H., and Coauthors, 2020: Evaluation of global ocean-sea-ice model simulations based on the experimental protocols of the Ocean Model Intercomparison Project phase 2 (OMIP-2). *Geoscientific Model Development*, **13**, 3 643–3 708, https://doi.org/10.5194/gmd-13-3643-2020.

Zhang, H. and Coauthors, 2020: CAS-ESM2: Description and Climate Simulation Performance of the Chinese Academy of Sciences (CAS) Earth System Model (ESM) Version 2.0. *Journal of Advances in Modeling Earth Systems*, http://doi.org/10.1029/2020MS002210.